Showcasing research from Professor Crick's laboratory, School of Engineering and Materials Science, Queen Mary University of London, London, UK.

Investigating the viability of sulfur polymers for the fabrication of photoactive, antimicrobial, water repellent coatings

Sulfur polymer-nanoparticle composites are shown to facilitate a dual-action antifouling. This includes the repulsion and chemical breakdown of surface contaminants. This material's functionality is so potent that water droplets form spheres on the surface, while degradation of the waterborne components is still achieved. In the reported work, the material's dual-action antifouling functionality is demonstrated using chemical and biological fouling agents. This class of materials show the potential to be implemented as an approach for keeping a range of surfaces clean solely by interaction with either water or light.

As featured in:

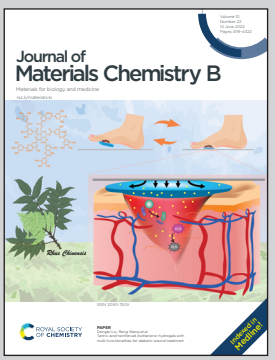

See Colin R. Crick *et al.*, *J. Mater. Chem. B*, 2022, **10**, 4153.

ROYAL SOCIETY OF CHEMISTRY

rsc.li/materials-b

Registered charity number: 207890

Journal of Materials Chemistry B

ROYAL SOCIETY OF CHEMISTRY

PAPER

View Article Online
View Journal | View Issue

Cite this: J. Mater. Chem. B, 2022, 10, 4153

Investigating the viability of sulfur polymers for the fabrication of photoactive, antimicrobial, water repellent coatings†

Rebekah L. Upton, [ab] Romy A. Dop, [a] Emma Sadler, [b] Amy M. Lunt, [a] Daniel R. Neill, [c] Tom Hasell [a] and Colin R. Crick *[b]

Received 11th February 2022,
Accepted 10th April 2022

DOI: 10.1039/d2tb00319h

rsc.li/materials-b

Elemental sulfur (S_8), a by-product of the petroleum refining industries, possesses many favourable properties including photocatalytic activity and antibacterial activity, in addition to being intrinsically hydrophobic. Despite this, there is a relative lack of research employing elemental sulfur and/or sulfur copolymers within superhydrophobic materials design. In this work, we present the use of sulfur copolymers to produce superhydrophobic materials with advanced functionalities. Using inverse vulcanization and the use of a natural organic crosslinker, perillyl alcohol (PER), stable S_8-PER copolymers were synthesised and later combined with silica (SiO_2) nanoparticles, to achieve highly water repellent composites that displayed both antimicrobial and photocatalytic properties, in the absence of carcinogenic and/or expensive materials. Here, we investigated the antibacterial performance of coatings against the Staphylococcus aureus bacterial strain, where coatings displayed great promise for use in antifouling applications, as they were found to limit surface adhesion by more than 99%, when compared to uncoated glass samples. Furthermore, UV dye degradation tests were performed, utilizing the commercially available dye resazurin, and it was shown that coatings had the potential to simultaneously exhibit surface hydrophobicity and photoactivity, demonstrating a great advancement in the field of superhydrophobic materials.

Introduction

Extremely water repellent materials display many remarkable properties, enabling them to produce functional coatings that are of significant scientific and industrial interest. Superhydrophobic functionalities include self-cleaning,[1–3] water purifying,[4–6] anti-bacterial,[7,8] and drag-reducing.[9,10] To date, many research efforts have been focused primarily on enhancing the physical durability of materials, as such small scale features often lead to mechanically weak microstructures. However, with growing environmental concerns, significant effort is now being focused on increasing the sustainability of fabrication approaches. By incorporating naturally occurring materials and/or waste by-products into established fabrication processes, superhydrophobic materials can be manufactured in a more environmentally friendly way.

Elemental sulfur (S_8, orthorhombic) is produced as a by-product of the petroleum refining industries. Its production (more than 60 million tonnes per annum) far exceeds its consumption, where it is mainly used for the production of sulfuric acid, a commodity chemical used for the synthesis of phosphoric fertilisers.[11,12] As such, elemental sulfur is an abundant and cheap material that has the potential to be utilized in new applications. Furthermore, sulfur possesses many commercially attractive properties, such as antibacterial activity, hydrophobicity and photocatalytic activity, making it a suitable choice for the design of functional materials.[13–15] The antibacterial properties of sulfur are well documented, showing a broad activity against both Gram-positive and Gram-negative species, including those associated with widespread antimicrobial resistance.[16,17] The precise mechanism is yet to be definitively established, however, multiple pathways have been proposed, including; binding to and inactivating enzymes containing –SH functional groups within the bacterial cells, crosslinking between sulfur-free radicals and proteins or lipids, and inhibition of bacterial virulence pathways.[18–20] Elemental sulfur is also known to be intrinsically hydrophobic, due to the

[a] University of Liverpool, Department of Chemistry, Materials Innovation Factory, Liverpool, L69 7ZX, UK
[b] Queen Mary University of London, School of Engineering and Materials Science, London, E1 4NS, UK. E-mail: c.crick@qmul.ac.uk
[c] University of Liverpool, Department of Clinical Infection, Microbiology and Immunology, 8 West Derby Street, Liverpool, L69 7BE, UK

† Electronic supplementary information (ESI) available. See DOI: https://doi.org/10.1039/d2tb00319h

lack of polar chemistry, and has also been reported to be photocatalytically active under both visible and UV radiation.[15] Interestingly, despite showing photactivity, Lantos *et al.* reported the use of elemental sulfur within silver/titanium dioxide (TiO_2) composites as a non-photodegradable filler, highlighting sulfur as a material that can retain its hydrophobic nature.[21]

In recent years, there has been growing interest in producing functional materials from sulfur, in order to exploit its inherent properties and utilise waste stockpiles. However, processing of elemental sulfur can often present challenges; at temperatures exceeding 159 °C, sulfur is known to self-polymerise *via* ring-opening polymerisation, resulting in a homopolymer that is unstable and susceptible to depolymerisation back to S_8 rings, upon cooling. Therefore, limiting its useability. However, inverse vulcanisation, a process first reported by Pyun *et al.* in 2013, offers a solution by stabilising sulfur chains to depolymerisation, achieved by reacting elemental sulfur with vinylic monomers (Fig. 1).[22] Inverse vulcanization is a bulk polymerisation process that is solvent-free and allows the synthesis of stable, high sulfur content polymers.[23] Furthermore, inverse vulcanized copolymers show promising applications across several fields, including improved cathode materials for Li-S batteries,[24] infrared transparent and highly refractive optical devices,[25,26] and for environmental remediation through mercury capture and oil–water separation.[27,28] Additionally, they have been reported to display antibacterial activity against *Escherichia coli*, *Staphylococcus aureus* and *Pseudomonas aeruginosa*, and thus, have the potential to be used in antibacterial applications.[16,29,30]

The use of sulfur-based compounds in the field of superhydrophobic materials has been previously reported, primarily through incorporation into synthetic coatings as nanoparticles, or the production of macromolecules and polymers *via* thiol–ene click chemistry.[21] Coatings prepared *via* thiol–ene click chemistry can form covalently bonded networks, and produce materials with high physical resilience.[31] However, in doing so, the functional properties of elemental sulfur are not readily transferred to the resultant materials. To our knowledge, inverse vulcanized copolymers have not been investigated for their use as superhydrophobic materials.

The research reported herein utilises sulfur-PER copolymers to produce superhydrophobic coatings that demonstrate both photocatalytic and antibacterial functionalities. The resulting copolymers were used in combination with SiO_2 nanoparticles as a roughening agent, to achieve coatings that were highly water repellent, displaying static contact angles up to 169° ± 1. The photocatalytic nature of the coatings was investigated by a series of dye degradation tests that demonstrated their ability to reduce resazurin dye under UV irradiation, in as little time as 40 minutes. Additionally, the antibacterial performance of coatings was assessed against the *S. aureus* bacterial strain, where coatings were found to significantly reduce bacterial surface adhesion/growth. To evaluate the real-world performance of materials, the UV stability of coatings was also probed (254 nm, 8 W), where it was shown that coatings were capable of maintaining surface hydrophobicity for 90 minutes under intense UV exposure. This research highlights the potential for a new class of more sustainable superhydrophobic polymer-nanoparticle composite materials, and evaluates the advanced functionalities that coatings can display, extending the real-world applicability of materials and promoting enhanced durability.

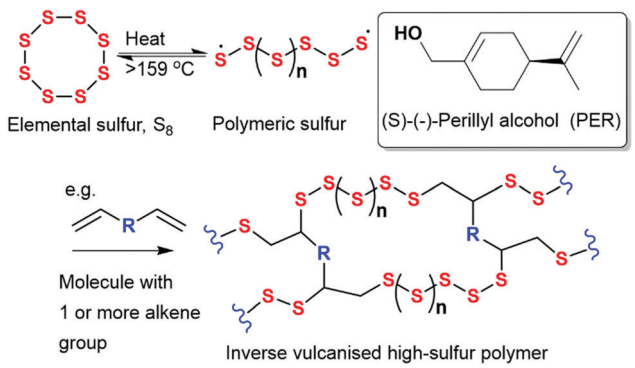

Fig. 1 General scheme for the synthesis of copolymers from elemental sulfur and simple organic crosslinkers *via* inverse vulcanization.

Experimental

Materials

Elemental sulfur (S_8, sublimed powder, reagent grade, ≥99.5%) was purchased from Brenntag UK & Ireland. Silicon dioxide nanopowder (SiO_2, 10–20 nm), hexamethyldisilazane (reagent grade, ≥99%), (S)-(−)-perillyl alcohol (≥95%), titanium dioxide (TiO_2, Aeroxide P25, 21 nm), 1H, 1H, 2H, 2H-perfluorooctyltriethoxysilane (FAS, 98%) and 2-hydroxyethyl cellulose (M_v 90 000) were purchased from Sigma Aldrich. Sylgard-1–84 (Silicone elastomer) was purchased from Ellsworth Adhesive Ltd. Resazurin (sodium salt, pure) was purchased from Acros Organics. Glycerol (99.5%) was purchased from Alfa Aesar. Tetrahydrofuran (THF, 99+ %, extra pure, stabilized with BHT), toluene (99.8+ %), chloroform ($CHCl_3$, 99.8%) and ethanol (analytical reagent grade) were purchased from Fisher Scientific Limited. Luria–Bertani broth (Miller), LB agar and phosphate-buffered saline (PBS) were purchased from Sigma-Aldrich. Methicillin-resistant *S. aureus* strain USA300 was cultured from frozen stocks stored at the University of Liverpool.[32]

Synthesis of sulfur-PER copolymers

Elemental sulfur was heated to >170 °C with continuous magnetic stirring. Once fully molten (visible by a change in appearance from a pale yellow powder to yellow/orange liquid), perillyl alcohol (PER) was added. The ratio of elemental sulfur: PER comonomer was varied in the experiments from 50 : 50 to 90 : 10, however, the total mass of the reaction remained at 15 g. The solution was left to stir at 800 rpm for 20–25 minutes until the reaction was almost at completion. The pre-polymer was then transferred into a silicone mould and left to cure at 140 °C for 18 hours.

Hydrophobization of SiO_2 nanoparticles

A solution of hexamethyldisilazane (HMDS, 1 mL) in toluene (100 mL) was added to a suspension of as-received silica

nanoparticles (10 g) in toluene (250 mL) and refluxed at 120 °C for 24 h, with magnetic stirring. Functionalized nanoparticles were then centrifuged and washed once in toluene and twice in ethanol (2000 rpm for 10 min per wash), before being dried in the oven at 80 °C overnight.

Preparation of composite coatings

Formulations comprising of solvent, sulfur polymers and silica nanoparticles as detailed below were sonicated and deposited onto glass slides by spray coating (Fig. 2) using a compression pump and airbrush gun (Voilamart), at a pressure of 2 bar. The airbrush was used at a distance of ~4 cm from the substrate and coated three times to ensure even coverage.

Sulfur-PER-SiO_2

PER polymer (PER_50, PER_60 and PER_70) were finely ground using a pestle and mortar before dissolving in chloroform (30 mL). Varying weight percentages of HMDS-functionalised SiO_2 nanoparticles (30–90% Wt% SiO_2) were then added to the suspension and continuously stirred for 2 hours before deposition at 60 °C, to facilitate solvent removal.

SiO_2-PDMS

PDMS (0.2905 g) was dissolved in n-hexane (30 mL), with the aid of mechanical stirring. HMDS-functionalised SiO_2 nanoparticles (0.2 g, 15 nm) were added and the suspension was left to stir for three hours. The deposition was carried out in ambient conditions, after which samples were left for 48 hours to cure.

Material characterisation techniques

Scanning electron microscopy (SEM) images were obtained using a Tescan FIB SEM S8000G operating at an acceleration voltage of 5–10 kV. Samples were vacuum sputter coated in a thin layer of chromium using a Quorum S150T ES sputter coater to improve electrical conductivity inside the SEM. Fourier Transform Infrared (FTIR) measurements were taken using a Bruker Optics' Vertex 70 over a range of 500 to 4000 cm^{-1}. Nuclear Magnetic Resonance (NMR) samples were analysed using a Bruker Advance DRX (400 MHz) spectrometer using deuterated chloroform as the solvent, all experiments were carried out at room temperature. UV-Vis absorbance spectra were obtained using a Cary 5000 UV-Vis-NIR Spectrometer in the range of 300–800 nm. Baselines were recorded for solid samples using a coated sample in the absence of any dye solution, and distilled water was used for liquid samples. Differential scanning calorimetry (DSC) measurements were performed on a TA instruments discovery series DSC 25, using a heat-cool-heat method with heating/cooling rates of 10 °C min^{-1}, from −80 to 150 °C. Powder X-ray diffraction (PXRD) measurements were collected in transmission mode on a Panalytical X'Pert PRO MPD equipped with a high throughput screening XYZ stage, X-ray focusing mirror and PIXcel detector using Cu Kα radiation. Data were recorded using loose powder samples held on thin Mylar film in aluminium well plates, over the range 4–40° in ~0.013° steps over 60 minutes. Static contact angle measurements were taken using a DSA100 Expert Drop Shape Analyser (Kruss GmbH) operating with Young-Laplace fitting and using 6 μL water droplets. Baselines were assigned manually to minimise errors caused by the software analysis. Tilting angles were recorded by tilting the surface at 2° s^{-1}, recording the angle at which the droplet began to roll. At least 5 contact/tilting angle measurements were taken and averaged for every reported contact/tilting angle. Finger-wipe testing was used to characterize the mechanical stability of the coating by scraping with a finger from one

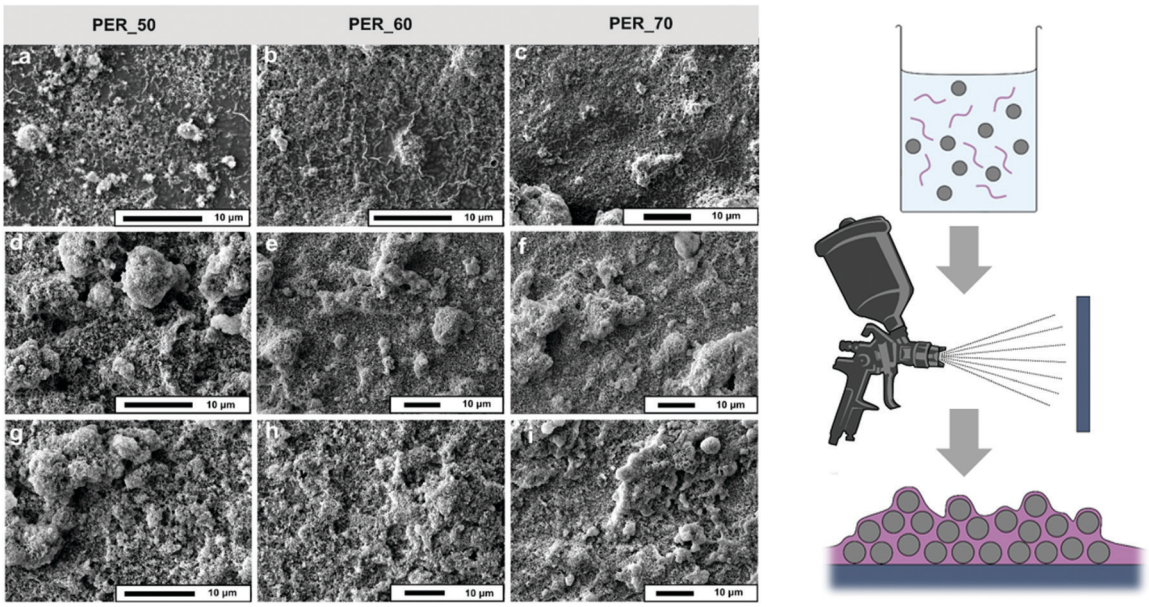

Fig. 2 (a–i) Top-down SEM micrographs showing the morphology of (a) PER_50–30, (b) PER_60–30, (c) PER_70–30, (d) PER_50–60, (e) PER_60–60, (f) PER_70–60, (g) PER_50–90, (h) PER_60–90 and (i) PER_70–90. Scale bars are shown. (J) Schematic of coating on substrate.

side of the material to the other. The change of CA was then measured at 5 different areas to qualitatively characterize the stability.

Solubility studies

PER polymers (100 mg, PER_50, PER_60, PER_70, PER_80 and PER_90) were weighed out in triplicate, into pre-weighed vials. Chloroform, tetrahydrofuran and toluene (5 mL) were added to a sample of each copolymer, and the polymer was sonicated to ensure complete dissolution, before being left to stir under ambient conditions for 2 hours. Following this, the solution was pipetted through a filter into a new pre-weighed vial and left under ambient conditions in the fume hood for 48 hours to allow for solvent evaporation. Before weighing, the vials were heated in the oven for a further 2 hours (above the boiling point of each solvent), to ensure complete solvent removal. The mass of the polymer and vial was weighed and subtracted from the initial vial mass, allowing for the weight percentage of recovered polymer to be determined. Any loss of soluble material within the filter was negligible and all samples were carried out in triplicate.

Dye degradation

An aqueous solution of resazurin dye was prepared (1 mg in 20 mL distilled water), sixteen droplets of which (20 μL each) were placed on the samples before exposure to UV radiation (254 nm) for a stated period of time. The samples themselves were positioned in containers 6.8 cm below a Spectroline ENF-280c UV lamp ($\lambda \sim 254$ nm, 8 W power), which emitted radiation *via* a 20 × 5 cm cut out rectangle in the container. After exposure, four droplets were removed from the surface using a pipette and dispensed into a demountable cuvette to allow for the absorbance spectra to be recorded. This process was repeated in 10-minute intervals (up to 40 minutes total exposure), with distilled water being used at the baseline. All testing was carried out in triplicate.

Antimicrobial testing

Methicillin-resistant *S. aureus* strain USA300 cultures obtained from glycerol stocks were cultured on lysogeny broth (LB) agar plates and incubated at 37 °C overnight.[33] A single colony was inoculated in 10 mL liquid LB followed by overnight incubation at 37 °C. After the incubation period, the Miles and Misra method was used to enumerate colony-forming units (CFU) of stocks by serial dilution with phosphate-buffered saline (PBS).[34] Cultured LB broth diluted to 10^5 CFU mL^{-1} (OD600 = 0.001) was added to a 24-well plate containing 1 × 1 cm^2 square samples and uncoated glass as the negative control. Samples were incubated for 5 h at 37 °C, after which the surrounding bacterial solution was removed. Viable cells in the removed solution were enumerated using the Miles and Misra method and PBS diluent. To enumerate cells adhered to the sample surfaces, the samples were rinsed with 1 mL of PBS to remove any planktonic cells before vortexing in 1 mL of LB broth for 10 s to remove any adhered cells.

Results and discussion

Synthesis and characterization of sulfur polymers

Perillyl alcohol (PER) is a monocyclic terpene that is found naturally in many essential oils, including those of citrus fruits.[35] In 2018, Parker *et al.* reported the synthesis of high sulfur content polymers *via* inverse vulcanization of elemental sulfur and perillyl alcohol.[36] The produced sulfur-PER copolymers in this study were synthesised to investigate their stability and properties, where the reported copolymers were found to display good solubility.[16,36] Therefore, to enhance the processability of elemental sulfur, which is known to show low solubility in all common organic solvents, inverse vulcanisation using the organic monomer PER was used as a method of promoting polymer solubility – a key requirement for superhydrophobic materials design. Copolymers were synthesised with compositions that spanned 50–90 wt% elemental sulfur (termed PER_50, PER_60, PER_70, PER_80 and PER_90), to investigate the effects that the crosslinker content had on polymer stability. Fourier-transform infrared (FTIR) spectroscopy was used to detect the physical crosslinking within the polymer matrix, between sulfur chains and organic PER molecules. The FTIR spectra of copolymers (PER-50 : PER-90, Fig. S1, ESI†) displayed a reduction in the intensity of C=C–H stretching (3082 cm^{-1}) and C=C stretching (1643 cm^{-1}) signals, in addition to the appearance of signals that corresponded to C–S bonds (704 cm^{-1}) – which were not present in the spectrum of pure PER. Thus, indicating that reaction had taken place between the crosslinker and elemental sulfur, due to a reduction in unsaturated hydrocarbons and the formation of C–S bonds. ^{1}H NMR spectroscopy was also used to compare the alkene units present in the unreacted PER and the resultant polymers (Fig. S2, ESI†). Loss of peaks corresponding to vinylic and allylic protons suggests consumption of alkene units in the monomer. The broad peaks remaining in the products are consistent with polymeric material, and the appearance of peaks at 3.5–4.0 ppm with H–C–S positions. Further characterisation was carried out using differential calorimetry (DSC) (Fig. S3, ESI†) and powder x-ray diffraction (PXRD) (Fig. S4, ESI†) to show if the copolymers were stable and uniformly reacted, as these techniques could highlight the presence of elemental sulfur that may have leached from the polymer. The DSC curves indicated that with a decreasing weight percentage of PER crosslinker, the copolymer became less stable, as crystalline sulfur could be detected (~105–115 °C) for both PER_80 and PER_90, likely as a result of depolymerisation overtime. PER_50, PER_60 and PER_70 had no peak representative of crystalline sulfur and appeared to be stable. These observations are consistent with the results obtained by Parker *et al.*, whereby inverse vulcanized polymers synthesised with PER were only stable with sulfur loadings of up to 70 wt%.[36] Glass transition temperatures (T_g) calculated from the curves were additionally shown to decrease with increased elemental sulfur content (T_g PER_50 = 26 °C, PER_90 = −25 °C), signifying that a higher weight percentage of crosslinker led to increased resistance to physical change, and a higher degree of branching/crosslinking.

PXRD indicated a similar trend, with signs of crystallinity being present for PER_80 and PER_90, appearing as the γ-polymorph as opposed to the α-polymorph (the most common polymorph of elemental sulfur) – suggested to be a result of the slow cooling of unstable sulfur within the polymer matrix. Furthermore, solubility studies were conducted for all copolymers (chloroform, THF and toluene, 100 mg/5 mL) where chloroform was determined to be the most successful solvent, demonstrating the highest mass percentages of recovered polymer across the range of copolymers examined; 97% ± 3 polymer for PER_50, 96% ± 3 for PER_60, 96% ± 3 for PER_70, 86% ± 5 for PER_80 and 77% ± 3 for PER_90. Polymer recovery was collectively lower for other trialled solvents, toluene and THF. The solubility of PER products in chloroform and THF are indicative of polymers that are not fully crosslinked. It is possible that PER can undergo hydrogen abstraction during inverse vulcanization with sulfur, to form aromatic units, which has been found for the structurally related limonene.[37] The aromatization would result in linear polymer units which would lower the crosslink density of the polymer and hence increase its solubility (Fig. S5, ESI†). ^{1}H NMR spectra obtained for sulfur-PER polymers (Fig. S2, ESI†) show weak signals in the aromatic region, indicative of some aromatization of PER.[36]

The wettability of each material was examined, where flat surfaces were used to avoid any intensification in contact angle, as a result of surface roughness. Smooth surfaces were achieved by melting a thin layer of sulfur/polymer onto a glass slide, or pellet pressing loose material, in the case of powdered sulfur. In line with the literature, α-sulfur was found to be hydrophobic, displaying a contact angle of 105° ± 2 for the pressed pellet sample, and a slightly lower contact angle of 98° ± 3 for the smooth sulfur surface (difference due to unavoidable surface roughness of pellet pressed surface). On the other hand, sulfur-PER copolymers exhibited collectively lower contact angles, showing a slight trend between increasing weight percent of sulfur and enhanced hydrophobicity (PER_50 76° ± 4, PER_60 80° ± 3, PER_70 78° ± 3, PER_80 76° ± 7, PER_90 82° ± 6, tilting angles all exceeded 90°). However, this cannot be said definitively, as the range of recorded static contacts for sulfur-PER polymers was very small, and values did not deviate significantly (76–82°). Although the chemical structure of PER primarily comprises hydrocarbons, it also contains a terminal hydroxyl group. Hence, this likely contributed to the overall decrease in contact angle for all sulfur copolymers, due to the introduction of polar groups. Furthermore, tilting angles were determined to be >90° in all cases, signifying that water droplets were fully adhered to the surface, exhibiting a Wenzel wetting state. This was unsurprising due to the intrinsic wettability of copolymers, and lack of surface roughness. However, it was anticipated that superhydrophobicity and a stable Cassie–Baxter wetting state could be attained if surface roughness was induced, due to polymers being situated on the border between hydrophilic and hydrophobic (90°).

Fabrication and characterization of Sulfur-PER-SiO_2 superhydrophobic coatings

A high level of surface roughness is a fundamental requirement to achieve surface superhydrophobicity. Hence, SiO_2 nanoparticles were introduced to obtain a textured surface, as they can easily be functionalised and are not activated under UV irradiation. As PER_80 and PER_90 were shown to have stability issues, these were not used to form SiO_2 composites, as it was anticipated that further processing would result in more excessive elemental sulfur leaching. PER_50, PER_60 and PER_70 were used to produce formulations that comprised various weight percentages of SiO_2 nanoparticles (30–90 wt% SiO_2), to assess the morphologies and resultant static/dynamic wetting properties. From scanning electron microscopy (SEM) imaging, it became apparent that various microstructures were obtainable for coatings that comprised different sulfur-PER copolymers, while also varying for different SiO_2 weight percentages (Fig. 2).

When a reduced loading of SiO_2 nanoparticles was employed, excess polymer was visible and surface roughness was compromised. Furthermore, some order of phase separation between polymer and particles appeared to occur for coatings with a low SiO_2 content and high percentage of crosslinker (likely due to the presence of more polar groups), resulting in dense polymer regions and/or large uncoated SiO_2 aggregates (Fig. S6, ESI†). However, uniformity improved with higher loadings of SiO_2 nanoparticles, with coatings containing > 50 wt% SiO_2 showing no visible flattened polymer regions or polymer-particle separation. Despite initial results indicating PER_70 to be stable (*via* DSC and PXRD), elemental sulfur appeared in SEM micrographs of all surfaces fabricated from PER_70 (Fig. S7, ESI†). Here, it was anticipated that the sulfur content may have been too high to endure re-processing of the material, and so subsequently led to precipitation of crystalline sulfur particles. Crystalline elemental sulfur was not present for PER_50 and PER_60, suggesting that these polymers were stable during re-processing and could be successfully employed to produce superhydrophobic coatings. Static and dynamic wettability measurements were taken to observe any trends in surface hydrophobicity between different Sulfur-PER-SiO_2 surfaces. As expected from the SEM micrographs, the samples containing low SiO_2 weight percentages resulted in reduced surface roughness, relatively low static contact angles (≤120°) and high tilting angles (>90°), when compared to their higher weight percentage equivalents. When the SiO_2 content increased, hierarchical surface roughness was enhanced (confirmed *via* SEM), therefore, increasing the ability to trap air within the surface features and promoting Cassie–Baxter wetting, as interactions between water droplets and the surface were minimised. The highest contact angle was observed for PER_70–90 (10 wt% PER_70/90 wt% SiO_2, 169° ± 1), where it was found that increasing the sulfur content generally resulted in a higher static angle *i.e.*, PER_70 > PER_60 > PER_50. It was anticipated that the leaching of elemental sulfur particles might have attributed to an enhancement in surface roughness for coatings fabricated from the PER_70 copolymer. PER_60–60 coatings were found to display moderate resilience when subject to a finger wipe test, exhibiting a static contact angle of 146° ± 4 after light abrasion. This was comparable to SiO_2-PDMS coatings reported in our previous work, where polymer-nanoparticle composites were found to show

superior resilience to molecular composites, due to having stronger particle–particle interactions and greater binding strength to the underlying substrate.[38] It is suspected that this arises from the extensive polymer network that surrounds nanoparticles, taking on the role of a polymeric adhesive and resulting in greater intermolecular interactions. However, the physical resilience of coatings is still very limited when considering real-world applications, and further research would be required to elevate the abrasion resistance of coatings *e.g.*, the introduction of high-strength additives or a more extensively crosslinked polymer.

Resazurin dye degradation testing

Resazurin is a commercially available redox dye, that when in an aqueous solution, is an intense blue colour. Upon undergoing photo-reduction in the presence of a photocatalyst, the dye is irreversibly reduced to resorufin (Fig. S8, ESI†), with a visible colour change from blue to pink. The degradation of resazurin dye generally occurs due to reduction by generated radical species, in which photogenerated holes within the dye undergo an irreversible reaction with the sacrificial electron donor – the full degradation mechanism has been previously reported by Kafizas *et al.*[39] As discussed, superhydrophobic wetting minimises the liquid–solid contact as a result of the air-layer trapped within the rough surface morphology, water still remains in contact with the tops of surface features and so will allow for the passage of radicals at these points leading to the degradation of the dye. Here, a series of dye degradation tests were carried out to investigate the photocatalytic behaviour of coatings; a total of sixteen 20 μL droplets of aqueous dye (1 mg resazurin in 20 mL distilled water) were deposited onto each sample and exposed to set intervals of UV radiation (254 nm, 8 W). Four droplets (to allow for increased surface-droplet contact) were pipetted into a demountable cuvette at 10-minute time intervals, and the UV-Vis absorbance spectrum of the aqueous dye was recorded to track photo-reduction. To assess the stability of the dye under intense irradiation, before testing with photoactive coatings, SiO_2-PDMS samples were employed. Fig. 3 shows that no shift peak can be seen from 602 nm to lower wavelengths and that peak flattening at 380 nm did not occur over the 40-minute irradiation period (expected peak shifts when reazurin is photo-reduced to resorufin), indicating that the dye solution was relatively stable when exposed to 254 nm radiation across the testing period. The variation in peak height of both peaks could be explained by a difference in dye concentration/volume, and the method used to collect the testing samples. Furthermore, the dye retained its intense blue colour, and so it could be said that no significant interference/chemical reduction of the dye was occurring in the absence of a photoactive material. Hence, any observed degradation could be attributed to a photocatalysis mechanism.

Further tests were carried out using elemental sulfur (obtained from melting and manually spreading molten sulfur across a glass slide) and PER_60–60 coatings (40 wt% PER_60/60 wt% SiO_2). PER_60–60 was selected as the optimal coating due to its stability and extreme water repellence (exhibiting a stable Cassie–Baxter wetting state, contact angle of 166° ± 2 and tilting angle of 9° ± 2), while still containing a substantial polymer content. From Fig. 4a and b, reductions in the peaks at ~602 nm and ~380 nm and enhancements at ~572 nm and ~532 nm were visible in both samples after exposure to UV radiation (254 nm, 8 W) – evidence for the reduction of resazurin to resorufin; this was further confirmed by the visual colour change (see Fig. 4d and Fig. S9, ESI†). Elemental sulfur appeared to be more photocatalytic efficient during the 40-minute exposure period. This was highlighted by a greater decrease in peak height on the UV-Vis spectrum, where peaks were observed to reduce by 88% (602 nm: 572 nm) and 86% (380 nm: 362 nm), compared to PER_60–60, where peak height was seen to reduce by 84% (602 nm: 572 nm) and 77% (380 nm: 362 nm). Nonetheless, the performance of PER_60–60 was comparable, despite containing just 40 wt% sulfur-PER polymer. To confirm that the dye was being reduced by photogenerated species, and not chemically reacting with the surface, droplets were deposited on the surface of PER_60–60 and samples were kept in the dark (having avoided light exposure 7 days prior to use, see Fig. 4c). A small decrease in peak height at 602 nm was observed, but no significant decrease in peak height at 380 nm was found to take place. Again, this could be explained by differences in concentration/volume of dye during the exposure period. However, the possibility of the chemical reduction of dye molecules, initiated through interactions with the sulfur polymer surface, cannot be fully excluded. Although, within the given exposure period, there did not appear to be significant interference/chemical reduction of the dye, and therefore, it was deduced that any substantial photoreduction is likely due to a photocatalysis mechanism.

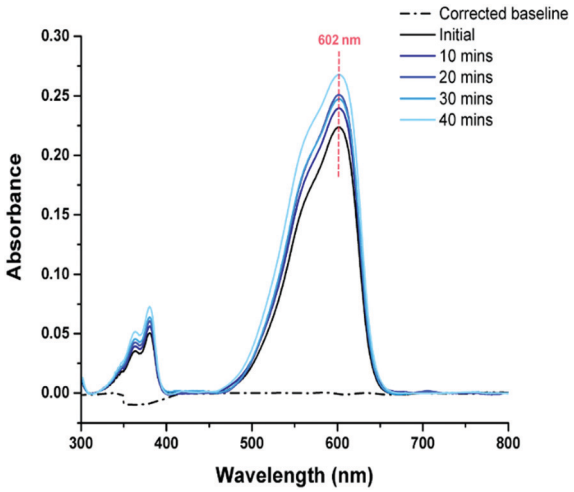

Fig. 3 Overlaid UV-Vis absorbance spectra of aqueous resazurin dye droplets (1 mg per 20 mL), removed from the surface of SiO_2-PDMS after each 10 minute irradiation interval, up to 40 minutes of UV exposure (254 nm, 8 W). The highlighted absorption peak is at 602 nm, showing that no peak shift has occurred over time. All spectra have been baseline corrected.

UV stability

The UV stability of elemental sulfur (7 mm diameter pressed pellets) was initially tested to monitor any immediate changes

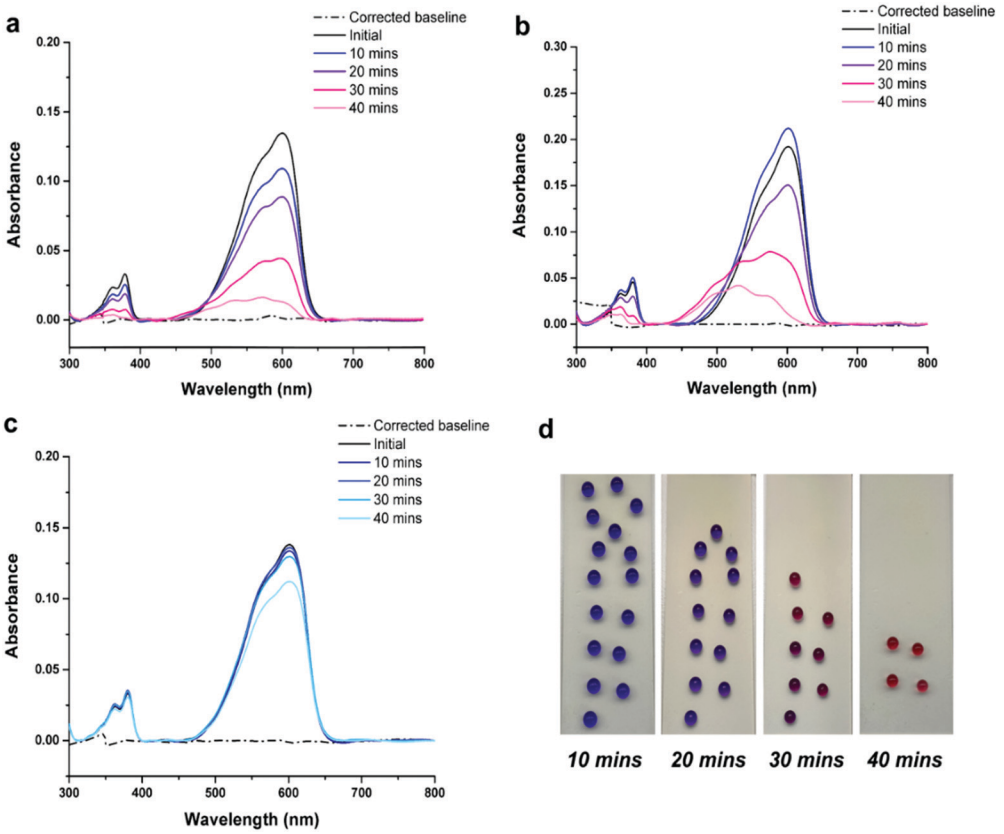

Fig. 4 Overlaid UV-Vis absorbance spectra of aqueous resazurin dye droplets (1 mg per 20 mL), removed from the surface of (a) flat elemental sulfur, (b) PER_60–60 under standard conditions (254 nm, 8 W) and (c) PER_60–60 when left in the dark. (d) Digital images of dye droplets on the surface of PER_60–60 after exposure to 10–40 minutes of UV (left to right, 254 nm). All spectra have been baseline corrected.

in surface chemistry. Both static and dynamic wettability measurements were recorded every 30 minutes up to 90 minutes, and every hour thereafter. Through the entire testing period (4.5 hours) the sulfur remained hydrophobic, with very little variation between measurements, showing excellent stability against UV irradiation. PER_60–60 was tested in the same manner and showed high stability for ~90 minutes before undergoing a complete wetting transformation from the Cassie-Baxter to Wenzel wetting state after 2.5 hours of irradiation. After the full 4.5 hours of exposure to UV irradiation (254 nm), PER_60–60 had decreased from an initial static contact angle of 166° ± 2 (tilt angle 9° ± 2) down to 51° ± 7. It is expected that intense UV exposure not only promotes photocatalysis but also degradation of the polymer and/or S–S bonds, leading to the production of organic contaminates that change the wettability and result in the UV-induced hydrophilicity that was observed.[40] As previously reported by Liu *et al.*, the suspected photocatalysis mechanism of elemental sulfur liberates $OH^{\bullet}$ radicals – though sulfur can retain its intrinsic hydrophobicity, the presence of radical species could contribute towards the degradation of the organic crosslinker.[40] Despite this, when compared to our past work using coatings composed of titanium dioxide nanoparticles functionalised with a monolayer of fluoroalkyl silane molecules (TiO2-FAS), which turned superhydrophilic after only 12 minutes of irradiation, PER_60–60 displayed greatly enhanced UV stability. It is expected that the presence of sulfur decelerated the rate of photodegradation due to its stability against UV induced changes in wettability. However, over time, the presence of organic contaminants, and breakdown of the PER crosslinker eventually lead to surface hydrophilicity. The degradation of PER crosslinkers (either full or partial) was confirmed *via* FTIR (Fig. S10, ESI†) where substantial peak reduction was observed as well as weakening of the Si–C stretching (~760 cm^{-1}), suggesting additional degradation of the hydrophobic $-CH_3$ groups that could further contribute to loss of hydrophobicity. The comparative stability of the pure sulfur to UV irradiation, as judged by the lack of change in WCA or TA (Fig. 5a), rather than indicating that the S–S bonds of S_8 are not affected, is more likely to reflect that S_8 is the most thermodynamically favourable form of elemental sulfur.[41] Although the UV stability results for elemental sulfur show minimal change, this does not indicate superiority for forming superhydrophobic materials, as they lack the processability associated with the crosslinked samples.

Antimicrobial testing of PER_60–60

The antibacterial properties of inverse vulcanized sulfur-PER polymers have been reported.[16] Copolymers were shown to have an inhibitory effect against both Gram-positive *S. aureus* and Gram-negative *P. aeruginosa*. In addition to this, polymers

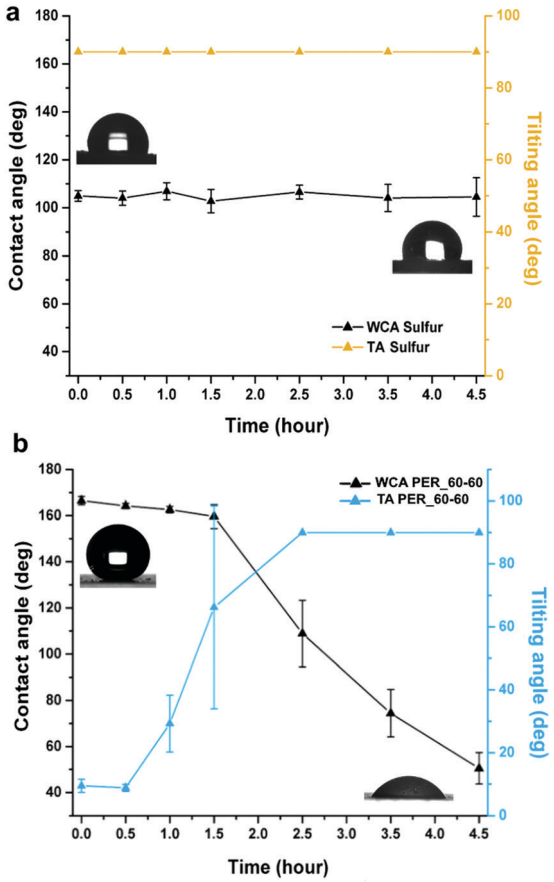

Fig. 5 The change in static contact angle and tilting angle with UV irradiation time (254 nm, 8 W) for (a) sulfur (7 mm diameter pellet, one measurement per pellet, total of 5 readings/pellets per data point) and (b) PER_60–60. Inset: Corresponding digital image of a water droplet on the surface of sulfur and PER_60–60 at 0 hours and 4.5 hours.

showed resistance to *S. aureus* and *P. aeruginosa* biofilm growth on their surfaces, relative to polypropylene.[16] Here, the antimicrobial activity of the superhydrophobic PER_60–60 sample was tested, to unveil if the antibacterial nature of the polymer was retained when formulated as a superhydrophobic coating on a glass substrate. The samples were tested using methicillin-resistant *S. aureus* USA300 and both solution and surface effects on bacterial growth/adhesion were investigated, using uncoated glass as a negative control. Additionally, SiO_2-PDMS, elemental sulfur and flat PER_60 polymer were also tested for comparative purposes.

A reduction in viable *S. aureus* colony forming units in solution was observed for sulfur-based materials, with elemental sulfur displaying a 24.6% reduction (0.12 log reduction, $p = 0.003$), flat PER_60 displaying a 58.1% reduction (0.38 log reduction, $p = 0.0007$), and superhydrophobic PER_60–60 showing a 62.5% reduction (0.43 log reduction, $p = 0.0007$), in comparison to uncoated glass (Fig. 6). This meant that the coatings had either inhibited the growth of bacteria within the solution or that a significant number had adhered to the surfaces, and hence, were not accounted for in solution. The difference in the reduction in viable *S. aureus* cells in solution

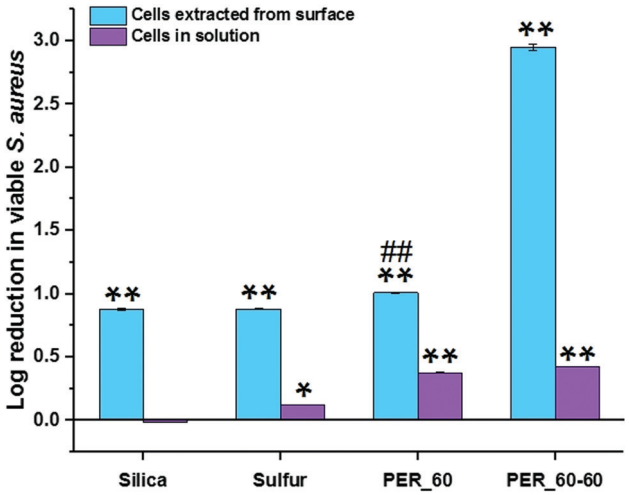

Fig. 6 A summary of the log reduction in viable *S. aureus* colony forming units extracted from the surface and from solution relative to uncoated glass for SiO_2-PDMS, elemental sulfur, PER-_60, and PER_60–60. $^{*}p < 0.05$ relative to uncoated glass, $^{**}p < 0.001$ relative to uncoated glass and $^{\#\#}p < 0.001$ for PER_60 compared to PER_60–60. The bacterial densities on the surface of uncoated glass and in the surrounding solution were 1.1×10^7 and 1.6×10^8, respectively All samples were tested in technical triplicate and the standard deviation was used to define the error bars.

for PER_60 compared to PER_60–60 was not statistically significant ($p = 0.2$). When compared with the non-sulfur containing superhydrophobic SiO_2-PDMS sample, however, the benefit of the added sulfur becomes apparent. A negligible difference was observed in viable *S. aureus* cells in solution for SiO_2-PDMS samples, due to the absence of the intrinsic antibacterial properties present by sulfur. When surface adhered bacteria were quantified, an even larger fold reduction was observed, suggesting that both SiO_2-PDMS and sulfur-based coatings are antibacterial. *S. aureus* colony forming units extracted from the surface of elemental sulfur displayed an 86.8% reduction (0.88 log reduction, $p = 0.0006$), PER_60 polymer showed a 90.3% reduction (1.01 log reduction, $p = 0.0005$) and PER_60–60 showed a 99.89% reduction (2.95 log reduction, $p = 0.0001$), relative to uncoated glass. Unlike in solution, SiO_2-PDMS sample displayed a significant reduction in adhered cells, showing an 86.8% reduction (0.88 log reduction), relative to uncoated glass.

As the bacteria were in an aqueous solution, the superhydrophobic samples were significantly more effective in reducing bacterial attachment and growth at the surface, due to their extreme water-repelling properties. Additionally, there is a reduced surface area for bacterial attachment and nucleation points, as a result of the Cassie–Baxter wetting state (trapped air leading to minimal solid-water interface), which likely accounts for the higher percentage reduction on the surface. This, in combination with the ability of sulfur to kill bacteria, suggested to occur *via* homolytic S–S bond cleavage of polysulfide linkages by Smith *et al.*,[30] led to a triple-action antibacterial effect and the superior surface reductions in bacterial numbers shown by PER_60–60, compared to superhydrophobic SiO_2-PDMS and sulfur samples, which were statistically significant compared with PER_60 ($p = 0.0008$).

Conclusions

Herein, we report the novel synthesis of superhydrophobic coatings, comprising sulfur-PER copolymers and SiO_2 nanoparticle composites, that displayed stable Cassie–Baxter wetting with reported static contact angles of up to $169^\circ \pm 1$ (tilt angle $6^\circ \pm 3$). Though high sulfur content polymers appeared to be unstable due to the detection of elemental sulfur ($\geq$70 wt% sulfur), PER_50 and PER_60 were shown using a series of characterisation techniques to be stable, even after reprocessing. Following this, PER_60–60 was selected as a representative coating to undergo functional examination to probe its photocatalytic behaviour, UV stability and antibacterial properties. During exposure to intense UV irradiation (254 nm, 8 W), the coating was shown to reduce the commercially available resazurin dye within 40 minutes, having a comparable activity to that of flat elemental sulfur, where photocatalysis was determined to be the principle mechanism of degradation. Although the UV stability of the PER_60–60 coating was initially found to be high, maintaining its superhydrophobic nature for $\sim$90 minutes, after this point a considerable decline was observed, whereby materials underwent a wetting state transition and adopted a Wenzel wetting state. Though it is assumed that this UV-induced change in surface wettability occurred due to photodegradation of the organic crosslinker, the initial stability is expected to be as a result of the non-photodegradable nature of elemental sulfur (dynamic reversible nature of S–S bonds),[26] allowing it to have superior UV stability when compared to generic photoactive superhydrophobic materials (TiO_2-based composites). Furthermore, the antibacterial performance of PER_60–60 was assessed, where it was found to display a 99.89% reduction in bacterial surface growth/adhesion, when compared to plain glass. Here, a combination of limited contact area for bacterial growth, due to the presence of interfacial air pockets, and the intrinsic antibacterial nature of sulfur copolymers themselves, was suspected to significantly enhance the antibacterial properties of superhydrophobic sulfur-PER-SiO_2 coatings.

The reported work paves the way for further investigation into sulfur-based superhydrophobic materials and provides more sustainable raw materials options for superhydrophobic materials design, offering alternatives to the potentially carcinogenic and expensive metal/metal oxides that are frequently employed to impart photocatalytic and/or antibacterial properties (*e.g.* TiO_2/silver). Furthermore, this work indicates potential for future development, primarily in the consideration of using more chemically robust organic crosslinkers, which could potentially enhance the overall UV stability of the coatings, and increase the longevity of the desired functionalities. These coatings show promise for implementation in a range of applications, particularly anti-fouling coatings/materials.

Author contributions

R. L. U., E. S., and C. R. C. led on the project conceptualisation, investigation, methodology development, validation, visualisation and writing with help from R. A. D., D. R. N and T. H., particularly with sulfur polymer preparation and bacterial studies. RLU was the principal lead for drafting the initial draft of the manuscript. R. L. U., E. S, R. A. D and A. L. were responsible for data curation and formal analysis, in their respective areas of investigation. CRC led on the funding acquisition, project administration, resources and supervision.

Conflicts of interest

There are no conflicts to declare.

Acknowledgements

The authors would like to thank the EPSRC for research funding. TH holds a Royal Society University Research Fellowship. The authors would like to thank Krzysztof Pawlak from The Materials Innovation Factory for his assistance with UV-Vis measurements.

References

1 R. L. Upton and C. R. Crick, *Mol. Syst. Des. Eng.*, 2020, **5**(4), 876–881.
2 Y. Lu, S. Sathasivam, J. Song, C. R. Crick, C. J. Carmalt and I. P. Parkin, *Science*, 2015, **347**, 1132–1135.
3 S. He, J. Shi, J. Huang, J. Hu, Y. Lai and Z. Chen, *Chem. Eng. J.*, 2021, **416**, 127768.
4 E. Sadler and C. R. Crick, *Sustainable Mater. Technol.*, 2021, **29**, e00321.
5 M. Khosravi, S. Azizian and R. Boukherroub, *Sep. Purif. Technol.*, 2019, **215**, 573–581.
6 Y. A. Mehanna and C. R. Crick, *Materials*, 2020, **13**(14), 3160.
7 E. Ozkan, C. C. Crick, A. Taylor, E. Allan and I. P. Parkin, *Chem. Sci.*, 2016, **7**, 5126–5131.
8 Z. Montgomerie and K. C. Popat, *Mater. Sci. Eng., C*, 2021, **119**, 111503.
9 H. Xu, C. R. Crick and R. J. Poole, *J. Mater. Chem. A*, 2018, **6**, 4458–4465.
10 Y. A. Mehanna, E. Sadler, R. L. Upton, A. G. Kempchinsky, Y. Lu and C. R. Crick, *Chem. Soc. Rev.*, 2021, **50**, 6569–6612.
11 M. S. Karunarathna, M. K. Lauer, T. Thiounn, R. C. Smith and A. G. Tennyson, *J. Mater. Chem. A*, 2019, **7**, 15683–15690.
12 D. A. Boyd, *Angew. Chem., Int. Ed.*, 2016, **55**, 15486–15502.
13 J. T. Weld and A. Gunther, *J. Exp. Med.*, 1947, **85**, 531–542.
14 S. M. Salehabad and S. Azizian, *ACS Appl. Mater. Interfaces*, 2020, **12**, 43201–43211.
15 G. Liu, P. Niu, L. Yin and H. M. Cheng, *J. Am. Chem. Soc.*, 2012, **134**, 9070–9073.
16 R. A. Dop, D. R. Neill and T. Hasell, *Biomacromolecules*, 2021, **22**, 5223–5233.
17 S. Saedi, M. Shokri and J. W. Rhim, *Arabian J. Chem.*, 2020, **13**, 6580–6588.

18 T. H. Jakobsen, M. Van Gennip, R. K. Phipps, M. S. Shanmugham, L. D. Christensen, M. Alhede, M. E. Skindersoe, T. B. Rasmussen, K. Friedrich, F. Uthe, P. Ø. Jensen, C. Moser, K. F. Nielsen, L. Eberl, T. O. Larsen, D. Tanner, N. Høiby, T. Bjarnsholt and M. Givskov, *Antimicrob. Agents Chemother.*, 2012, **56**, 2314–2325.
19 L. Libenson, F. P. Hadley, A. P. McIlroy, V. M. Wetzel and R. R. Mellon, *J. Infect. Dis.*, 1953, **93**, 28–35.
20 P. N. L. Lens and S. Saikia, Environmental Technologies to Treat Sulphur Pollution: Principles and Engineering, 2020.
21 E. Lantos, L. Mérai, Á. Deák, J. Gómez-Pérez, D. Sebők, I. Dékány, Z. Kónya and L. Janovák, *J. Mater. Sci. Technol.*, 2020, **41**, 159–167.
22 J. Lim, J. Pyun and K. Char, *Angew. Chem., Int. Ed.*, 2015, **54**, 3249–3258.
23 P. Yan, W. Zhao, B. Zhang, L. Jiang, S. Petcher, J. A. Smith, D. J. Parker, A. I. Cooper, J. Lei and T. Hasell, *Angew. Chem., Int. Ed.*, 2020, **59**, 13371–13378.
24 A. G. Simmonds, J. J. Griebel, J. Park, K. R. Kim, W. J. Chung, V. P. Oleshko, J. Kim, E. T. Kim, R. S. Glass, C. L. Soles, Y. E. Sung, K. Char and J. Pyun, *ACS Macro Lett.*, 2014, **3**, 229–232.
25 T. S. Kleine, T. Lee, K. J. Carothers, M. O. Hamilton, L. E. Anderson, L. Ruiz Diaz, N. P. Lyons, K. R. Coasey, W. O. Parker, L. Borghi, M. E. Mackay, K. Char, R. S. Glass, D. L. Lichtenberger, R. A. Norwood and J. Pyun, *Angew. Chem., Int. Ed.*, 2019, **58**, 17656–17660.
26 J. J. Griebel, N. A. Nguyen, S. Namnabat, L. E. Anderson, R. S. Glass, R. A. Norwood, M. E. Mackay, K. Char and J. Pyun, *ACS Macro Lett.*, 2015, **4**, 862–866.
27 D. J. Parker, H. A. Jones, S. Petcher, L. Cervini, J. M. Griffin, R. Akhtar and T. Hasell, *J. Mater. Chem. A*, 2017, **5**, 11682–11692.
28 M. J. H. Worthington, C. J. Shearer, L. J. Esdaile, J. A. Campbell, C. T. Gibson, S. K. Legg, Y. Yin, N. A. Lundquist, J. R. Gascooke, I. S. Albuquerque, J. G. Shapter, G. G. Andersson, D. A. Lewis, G. J. L. Bernardes and J. M. Chalker, *Adv. Sustainable Syst.*, 2018, **2**, 1800024.
29 Z. Deng, A. Hoefling, P. Théato and K. Lienkamp, *Macromol. Chem. Phys.*, 2018, **219**, 1–6.
30 J. A. Smith, R. Mulhall, S. Goodman, G. Fleming, H. Allison, R. Raval and T. Hasell, *ACS Omega*, 2020, **5**, 5229–5234.
31 C. E. Hoyle and C. N. Bowman, *Angew. Chem., Int. Ed.*, 2010, **49**, 1540–1573.
32 F. C. Tenover and R. V. Goering, *J. Antimicrob. Chemother.*, 2009, **64**, 441–446.
33 P. J. Planet, *J. Infect. Dis.*, 2017, **215**, S71–S77.
34 B. Y. A. A. Miles and S. S. Misra, *Epidemiol. Infect.*, 1931, **38**(6), 732–749.
35 T. C. Chen, C. O. da Fonseca and A. H. Schönthal, *Int. J. Mol. Sci.*, 2018, **19**, 1–21.
36 D. J. Parker, S. T. Chong and T. Hasell, *RSC Adv.*, 2018, **8**, 27892–27899.
37 J. A. Smith, X. Wu, N. G. Berry and T. Hasell, *J. Polym. Sci., Part A: Polym. Chem.*, 2018, **56**, 1777–1781.
38 R. L. Upton, Z. Davies-Manifold, M. Marcello, K. Arnold and C. R. Crick, *Mol. Syst. Des. Eng.*, 2020, **5**(2), 477–483.
39 A. Kafizas, D. Adriaens, A. Mills and I. P. Parkin, *Phys. Chem. Chem. Phys.*, 2009, **11**, 8367–8375.
40 Y. Li, Y. Li, Y. Liu, Y. Wu, J. Wu, B. Wang, H. Ye, H. Jia, X. Wang, L. Li, M. Zhu, H. Ding, Y. Lai, C. Wang, J. Dick and A. Lu, *Sci. Adv.*, 2020, **6**(47), eabc3687.
41 R. Steudel and B. Eckert, Solid Sulfur Allotropes, in *Elemental Sulfur and Sulfur-Rich Compounds I*, ed. R. Steudel, Topics in Current Chemistry, Springer, Berlin, Heidelberg, 2012, vol. 230, pp. 1–80, DOI: **10.1007/b12110**.

